Composite Poly(norbornene) Anion Conducting Membranes for Achieving Durability, Water Management and High Power (3.4 W/cm²) in Hydrogen/Oxygen Alkaline Fuel Cells

Garrett Huang,[1,*] Mrinmay Mandal,[1,*] Xiong Peng,[2,*] Ami C. Yang-Neyerlin,[3] Bryan S. Pivovar,[3,**] William E. Mustain,[2,**] and Paul A. Kohl[1,***,z]

[1]*School of Chemical and Biomolecular Engineering, Georgia Institute of Technology, Atlanta, Georgia, USA*
[2]*Department of Chemical Engineering, University of South Carolina, Columbia, South Carolina, USA*
[3]*Chemical and Materials Science Center, National Renewable Energy Laboratory, Golden, Colorado, USA*

Alkaline fuel cells and electrolyzers are of interest because they have potential advantages over their acid counterparts. High-conductivity anion conducting membranes were analyzed and used in alkaline hydrogen/oxygen fuel cells. The membranes were composed of reinforced block copolymers of poly(norbornenes) with pendant quaternary ammonium head-groups. It was found that membranes with light cross-linking provided excellent mechanical stability and allowed very high ion exchange capacity polymers to be used without penalty of excessive water uptake and swelling. The optimum membrane and fuel cell operating conditions were able to achieve a peak power density of 3.4 W/cm² using hydrogen and oxygen. The performance increase was greater than expected from minimizing ohmic losses. Mechanical deformations within the membrane due to excess water uptake can disrupt full cell operation. Cells were also run for over 500 h under load with no change in the membrane resistance and minimal loss of operating voltage.
© The Author(s) 2019. Published by ECS. This is an open access article distributed under the terms of the Creative Commons Attribution 4.0 License (CC BY, http://creativecommons.org/licenses/by/4.0/), which permits unrestricted reuse of the work in any medium, provided the original work is properly cited. [DOI: 10.1149/2.1301910jes]

Energy conversion devices using solid polymer electrolytes such as fuel cells and electrolyzers are promising options for producing and storing clean energy because of their high thermodynamic efficiency and solid-state design.[1] These devices are also scalable and can be used for transportation, remote and distributed power, and large-scale facilities for electricity and hydrogen production.

Polymer electrolyte membranes for fuel cells and electrolyzers are divided into two broad categories based on the dominant charge carrying ion: proton exchange membranes (PEMs) and anion exchange membranes (AEMs). There are already commercialized fuel cell electric vehicles and stationary power generators based on PEM membranes, however, there are significant costs associated with the platinum-based electrocatalysts and perfluorinated membranes. AEM-based devices have the potential to lower the cost of ownership compared to PEM-based devices because the high pH environment is advantageous for the oxygen reduction reaction (ORR, cathode reaction in AEM fuel cells) and oxygen evolution reaction (OER, anode reaction in AEM electrolyzers) kinetics, enabling the use of non-platinum catalysts.[2,3] Also, a variety of low-cost monomers can be used to synthesize hydrocarbon-based hydroxide ion conducting polymers that are stable in alkaline conditions, compared to the perfluorinated polymers needed for PEM-based electrochemical devices.[4,5] Perfluorinated polymers are expensive and present significant hazards due to monomer reactivity.

The critical metrics for AEMs include (i) high anion (e.g. hydroxide) conductivity, (ii) long-term alkaline stability at the AEM fuel cell operating temperature, (iii) robust mechanical properties for withstanding in-use pressure differences and avoiding polymer creep under compression, and (iv) control over excessive water uptake, which can disrupt ion transport within the electrodes and membrane.[5,6] There have been several reports of AEMs with hydroxide conductivity of over 100 mS/cm (60°C to 80°C).[7–12] More recent reports of AEMs have shown conductivity at or near 200 mS/cm (at 80°C).[7,13,14] High conductivity AEMs have been paired with optimized electrodes (with either platinum or non-platinum catalysts) to give AEM-based fuel cells with peak power densities exceeding 1 W/cm².[15–19] The current record for peak power in a hydrogen/oxygen AEM fuel cell is 2 W/cm².[20]

AEM fuel cells are known to be sensitive to the relative humidity of the fuel and oxidant streams, as well as the water uptake in the AEM and ionomer. Proper water management in the membrane and electrodes is critical to achieve high power density.[16] Water is electrochemically generated at the anode during the hydrogen oxidation reaction (HOR) and is consumed at the cathode by the ORR in an AEM fuel cell. Water is transported from the cathode to the anode by electro-osmotic drag and accompanying anion transport. Water also back diffuses from the anode to cathode. Without adequate water content within the membrane and electrodes, ionic conductivity suffers and polymer degradation accelerates due to the higher reactivity of hydroxide at lower water concentration. On the other hand, if there is too much water, catalyst layers can be easily flooded, and the efficient flow of ions within the electrodes and membranes can be disrupted. Mechanical degradation in the membrane can also occur due to the higher internal stress and expansion within the AEM. The conductivity, pH, and mechanical properties of the AEM are also affected by the presence of carbon dioxide in air because it forms bicarbonate and carbonate ions within the membrane. Fuel cell measurements are often made with CO_2-free air to avoid the complications of carbonate formation.[21] It is recognized that CO_2 uptake at the oxygen cathode can occur, which would lead to the formation of bicarbonate or carbonate in the membrane. The lower ion mobility for bicarbonate and carbonate compared to hydroxide results in higher ohmic losses within the anion conducting membrane and the possible accumulation of CO_2 in the hydrogen at the anode. Steps can be taken mitigate the negative effects of CO_2 at the air-cathode such as removing the CO_2 from air.

Efficient ion channels are needed in the AEM to achieve high conductivity because the number of ions cannot be independently increased (i.e. higher ion exchange capacity (IEC)) because of the penalty due to excessive water uptake. It has been shown that high mobility ion channels can be formed through the phase segregation obtained by the use of block copolymers (BCP).[22–24] Nanochannels have been created through nanophase separation between hydrophobic and hydrophilic blocks of a BCP.[25–27] It is important to note that not all BCP morphologies lead to high conductivity because the channels must also be interconnected for efficient ion conduction.[28]

The nature of the polymer backbone and type/location of hydrophilic groups within the polymer is important for long term AEM stability at high pH. It has been experimentally shown that polar moieties, such as ether, ketone or ester linkages, within the polymer or side-groups, are susceptible to nucleophilic attack and backbone

degradation.[29–31] Positioning the cation head groups at the ends of pendant alkyl tether has also been found to be an effective strategy for mitigating polymer degradation.[32] Quaternary ammonium head groups, especially the trimethyl ammonium cation, has been found to be have an excellent balance of conductivity and stability, although other conducting groups show merit as well.[10,33,34]

In this study, a BCP of poly(norbornene) (PNB) synthesized by vinyl addition polymerization has been used as the AEM. PNB is synthesized from an inexpensive precursor material (dicyclopentadiene), and has a high glass transition temperature (T_g). PNB also has an all-hydrocarbon backbone with compact monomer size, allowing for the creation of very high IEC AEMs.[7–9,35] This material was previously shown to form extremely stable polymers with moderate IECs of 1.55–2.60 meq/g.[9] Later, light cross-linking was used to control water uptake and provide additional mechanical strength without encountering the problems of high cross-link densities, resulting in polymers with even higher IEC (3.15–4.73 meq/g).[7,8] Additionally, thin membranes are desired to minimize ohmic losses in the AEM. A thin polytetrafluoroethylene (PTFE) reinforcement layer can be used when casting the membranes, making them mechanically tough.[36,37] In the past, similar approaches have been used to make composite AEMs for fuel cells that have achieved modest peak power densities of $<350\,mW/cm^2$.[38,39] The membranes used in this study use light cross-linking of a high IEC polymer to balance conductivity, water uptake and toughness to produce H_2/O_2 fuel cells with peak power density up to 3.4 W/cm^2 at 80°C using H_2/O_2. This is 70% higher than the previous highest reported H_2/O_2 AEM fuel cell to-date.[20] The membranes were also operated reliably for over 500 h (H_2/CO_2 free air) with no change in membrane resistance and minimal loss of operating voltage.

This study also shows the importance of minimizing excess water uptake. Light membrane cross-linking preserves efficient ion transport in the membrane and enables exceptionally high current density and power density fuel cell operation. The impact of dimensional stability on full-cell performance is much greater than simply the reduction of ohmic losses. Dimensional stability allows the efficient transport of anions throughout the entire membrane electrode assembly. This study opens the way for advances in low-platinum and non-platinum electrodes operating at high power.

Experimental

Synthesis of the tetrablock PNB copolymer GT64 with 64 mol% halogenated monomer was performed as previously reported by Mandal et al.[9] The IEC of the polymer was calculated based on ^{1}H NMR analysis using a Bruker Avance 400 MHz NMR instrument using CDCl$_3$ as the solvent as previously described.[7–9,11] The number average molecular weight (M_n) and dispersity (Đ) of the tetrablock copolymer were determined by gel permeation chromatography (GPC). GPC analyses were measured on a system composed of Shimadzu GPC units (DGU-20A, LC-20AD, CTO-20A, and RID-20A), a Shodex column (KF-804L), with HPLC grade THF (1 mL/min flow rate at 30°C) eluent and calibrated against a polystyrene standard as previously described.[7–9,11]

Light cross-linking was carried out by adding a cross-linking agent, N,N,N',N'-Tetramethyl-1,6-hexanediamine (TMHDA), to the polymer/solvent solution. The mole percent of TMHDA relative to the number of head-groups was: 2.5 mol%, 5 mol%, 10 mol%, 15 mol%, 20 mol% and 25 mol%. For example, GT64-5 has 5 mol% TMHDA with respect to the moles of head-groups within the BCP. The polymer solution was then solvent cast onto a PTFE reinforcement layer by Xergy, Inc. (Harrington, DE, United States) to form a composite film. The composite membranes were immersed in 50 wt% aqueous trimethylamine solution for at least 48 h at room temperature to convert the bromoalkyl tethers into quaternary ammonium head-groups. The quaternized membranes were washed thoroughly with DI water and stored in DI water until they were ready to be used.

The water uptake of the membranes was calculated according to Equation 1, where M_d is the dry mass of the membrane and M_w is the mass of the fully hydrated membrane after removing excess surface water.

$$WU\ (\%) = \frac{M_w - M_d}{M_d} \times 100 \quad [1]$$

The percent swelling was calculated by Equation 2, where V_d is dry volume of the membrane and V_w is the volume of the fully hydrated membrane after removing excess surface water.

$$Swelling\ (\%) = \frac{V_w - V_d}{V_d} \times 100 \quad [2]$$

The storage modulus of the reinforced composite membranes was measured by dynamic mechanical analysis (DMA) using a TA Instruments Q800 under a 1 Hz single-frequency strain mode in air at 30°C. A fully hydrated, rectangular sample was loaded into the DMA with tension clamps after removing surface water. Experiential parameters for the DMA were set to 0.1% strain and a preload force of 0.01 N with a force track of 125%.

Gas diffusion electrodes (GDEs) were prepared by hand spraying the catalyst layer onto a gas diffusion layer (GDL, Toray TGP-H-060 with 5% or 20% PTFE wetproofing) using a similar method described in Omasta et al.[19] ETFE-[poly(ethyene-co-tetrafluoroethylene)]-based radiation grafted AEI ionomer was provided by Varcoe and Poynton et al.[40] The ETFE AEI solid ionomer was finely ground with a mortar and pestle and then mixed with platinum on Vulcan carbon (Pt/C, Alfa Aesar HiSPEC 4000) to form the cathode catalyst ink mixture (20 wt% ionomer). Then, a small amount of DI water (1 ml) was added to the solid mixture and the mixture was ground for additional 10 minutes to avoid aggregated particles and then transferred to a vial. 2-propanol was added (a total of 9 ml) to the mortar to rinse the residual powder and then transferred to the mixture. The 2-propanol was added in 2 to 3 steps to ensure that the majority of the ink mixture was collected. The final ground ink mixture was sonicated with a sonic probe for 20 seconds followed by an additional 20 minutes of sonication in an ice bath before it was hand sprayed onto the GDL to produce one 25 cm^2 GDE. This process was repeated for the anode catalyst ink mixture using PtRu on Vulcan carbon catalyst with 8% PTFE (20 wt% ionomer). The platinum and platinum ruthenium metal loading of these GDEs were determined by X-ray fluorescence (XRF), reported in Table II. 5 cm^2 GDEs were cut from the larger Pt/C and PtRu/C 25 cm^2 GDEs, and combined with an oversized 5 cm^2 composite PNB AEM to assemble the MEAs.

The anode and cathode GDEs and membrane were ion exchanged in 1 M KOH solution for a total of 60 minutes (refreshing the base solution every 20 minutes) prior to cell assembly. The membrane was sandwiched between two GDEs and pressed together and secured in 5 cm^2 Fuel Cell Technologies hardware between two graphite single pass serpentine flow-fields and PTFE gaskets. The torque applied to the cell was 40 in-lb with a compression ratio of 25%.

The fuel cell was installed into the test station and operated at a cell temperature of either 60°C or 80°C. H_2 and N_2 was flowed through the anode and cathode, respectively, until the desired temperature was achieved. Once the desired temperature was reached, the N_2 was switched to O_2 and a constant voltage of 0.5V was applied to allow the cell to break-in. After a stable current density was established, the dew points of the anode and cathode reacting gases were optimized. After the cell was equilibrated at the set dew points, a polarization curve was measured by sweeping the voltage from OCV to 0.1 V at a 10 mV/s scan rate. Constant current density stability tests were performed at 600 mA/cm^2 in either O_2 or CO_2-free air; the resulting cell voltage was monitored over a minimum of 24 hours. A single H_2/CO_2-free air AEM fuel cell, assembled using the highest performing AEM, was subjected to long-term stability testing for more than 500 h. The dew points of the reacting gases were adjusted twice during this long-term durability test to ensure adequate membrane hydration.

High frequency resistance (HFR) was analyzed by electrochemical impedance spectroscopy (EIS) using a Metrohm Autolab potentiostat/galvanostat with booster at a constant current of 600 mA/cm^2 prior to cell polarization measurements. Cell temperature was either 60°C or 80°C with H_2 and O_2 or CO_2-free air flowed at the anode

Table I. Properties of composite crossed-linked poly(norbornene) AEMs.

Sample	Cross-linking (mol%)	IEC(meq/g)[a]	ASR(Ω-cm^2)[b]	Storage Modulus (MPa)[c]	Water Uptake (%)	Swelling (%)	IEC/ASR	WU/ASR
GT64-0	0	3.37	0.038	66.8	88	68	3.33	2316
GT64-2.5	2.5	3.36	0.056	75.4	82	45	3.30	1464
GT64-5	5	3.34	0.041	119	65	39	3.30	1585
GT64-10	10	3.31	0.033	129	35	24	3.28	1061
GT64-15	15	3.28	0.020	175	29	14	3.26	1472
GT64-20	20	3.25	0.025	458	24	11	3.23	968
GT64-25	25	3.22	0.025	553	18	7	3.20	735

[a]IEC calculated after the addition of TMHDA molecular weight; [b]Area specific resistance measured by EIS; [c]Storage modulus determined by DMA.

and cathode, respectively. Area specific resistance (ASR) of the membranes was calculated using the HFR. The hydrogen crossover rate was measured by from a linear voltage sweep from 0 to 0.5 V while H$_2$ and N$_2$ flowed at the anode and cathode, respectively. The cell temperature was set to 60°C with anode and cathode dew points set to 50°C.

Results and Discussion

The AEMs used in this study were composite films made of a high IEC, vinyl addition poly(norbornene) BCP solvent cast with a thin, polytetrafluoroethylene (PTFE) reinforcement layer from Xergy, Inc.[9] The PTFE reinforcement provides mechanical strength so that thin membranes (<20 μm) can be used. The same base polymer was used to make all composite membranes with the addition of different amounts of cross-linker, TMHDA. The polymer was synthesized according to a previous report and had a molecular weight (M_n) of 51.0 kDa with a dispersity (Đ) of 2.02.[7] This range of molecular weight and Đ was previously found to give membranes with high conductivity and good mechanical strength.[7,11] In a previous report, light cross-linking was found to be beneficial to the ionic conductivity of the membranes, especially for high IEC materials.[7] A high degree of cross-linking can inhibit ion mobility and cause brittleness. The optimum TMHDA concentration was studied by preparing composite AEMs with 0, 2.5, 5, 10, 15, 20 and 25 mol% TMHDA (i.e. mol% with respect to bromine head-groups within the polymer). The IECs of the cast polymer decreased slightly with TMHDA concentration due to the mass of the added TMHDA (3.37 to 3.28 meq/g), although the number of cation head-groups per monomer did not change. The properties of the membranes are summarized in Table I.

The mechanical properties of the membranes were influenced by the degree of cross-linking, Table I. The storage modulus and resulting stiffness of the membranes was improved by cross-linking. The uncross-linked membrane (GT64-0) had a storage modulus of only 66.8 MPa, which is similar to that of the PTFE by itself. Very light cross-linking (2.5 mol% TMHDA) led to a small increase in modulus to 75.4 MPa. There was an 8-fold increase in storage modulus

(553 MPa) for the membrane with the highest TMHDA concentration (25 mol%) compared to the uncross-linked sample. The higher modulus obtained with the cross-linked membranes provided rigidity and toughness so that they could be handled and used in very thin forms which minimized the ohmic losses during device operation.

The water uptake and swelling of the composite films decreased with TMHDA concentration, Table I. The water uptake and swelling were relatively high for the uncross-linked membrane, 88% and 68%, respectively. Even a very small TMHDA concentration (2.5 mol%) significantly lowered the swelling due to a more tightly bound structure within the cross-linked polymer network. At higher TMHDA concentrations, ≥10%, the water uptake and swelling were both well below 50%, which is advantageous for reducing the physical deformation when integrated into a membrane electrode assembly. The water uptake values are also clearly lower for the composite films than those of the free standing films without PTFE support, as reported previously.[7] For example, an unreinforced polymer membrane with 10 mol% TMHDA had 53% water uptake while GT64-10 had only 35% water uptake. At 20 mol% cross-linker, the effect is even more dramatic. The water uptake was 51% for the unreinforced membrane vs. 24% for the reinforced membrane. This shows that the hydrophobic PTFE reinforcement (as well as the cross-linking) contributes to limiting the water uptake in these membranes.

The HFR and ASR were evaluated using EIS. Figure 1 shows the Nyquist plots from the EIS measurements of MEAs at a cell temperature of 60°C with anode and cathode dew points set to 50°C (constant current of 600 mA/cm^2). The high frequency intercept (HFR) in the plots represents the total series ohmic resistance of the system (i.e. time-independent resistances without a parallel capacitance). The thinness of the membranes used here lowers the overall HFR, which helps to maximize fuel cell power output.

The ASR of the membranes was calculated from the HFR. This value represents the through-plane areal resistance of the membrane, which is especially important for composite membranes because the supporting material does not contribute to ionic conductivity. Through-plane hydroxide mobility depends on the orientation of the pores in the reinforcement layer and membrane packing. The ASR values for the

Table II. AEM fuel cell performance highlights at 60°C.

XL (mol%)	H$_2$ crossover (mA/cm^2)[a]	OCV (V)	A/C dew point (°C)	HFR (mΩ)[b]	Cell potential (V)	CD (mA/cm^2)	PPD (W/cm^2)	PtRu/C loading (mg/cm^2)[c]	Pt/C loading (mg/cm^2)[c]	Spec. power (W/mg PtRu)	Spec. power (W/mg Pt)	Spec. current (mA/mg PtRu)	Spec. current (mA/mg Pt)
0	40	0.881	50/50	7.6	0.555	2497	1.39	0.472	0.424	2.94	3.27	5291	5890
2.5	25	0.873	55/55	11.1	0.547	2270	1.24	0.331	0.313	3.75	3.97	6857	7251
5	5	0.950	48/52	8.1	0.554	3431	1.90	0.948	0.490	2.01	3.88	3620	7003
10	54	0.882	40/40	7.0	0.555	3417	1.89	0.730	0.515	2.56	3.68	4680	6634
15	12	0.930	40/40	6.2	0.537	4097	2.20	0.986	0.560	2.23	3.93	4155	7316

[a]Hydrogen crossover measured by EIS; [b]High frequency resistance measured by EIS; [c]Metal loadings for specific power and current determined by XRF. All other values measured or calculated based on test station data. XL = cross-linker concentration; A/C = denotes anode (A) and cathode (C) dew points in degrees Celsius, respectively; CD = current density; PPD = peak power density.
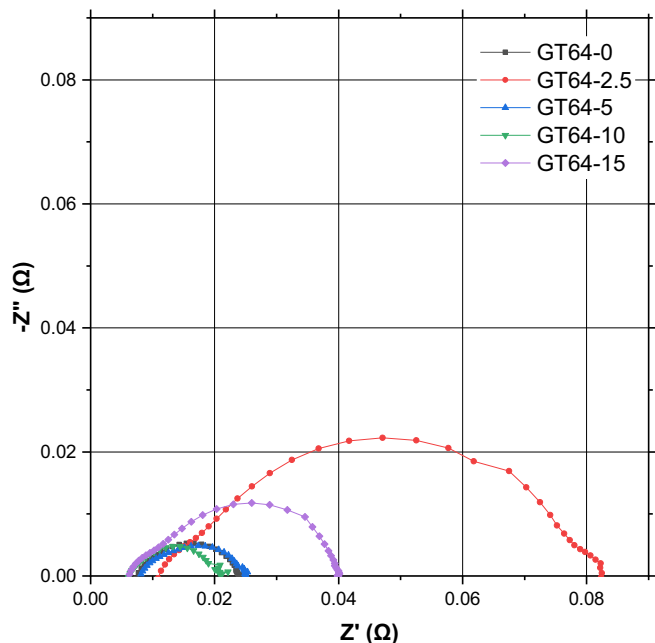
Figure 1. Nyquist plots of EIS measurements using five GT64 membranes with 0, 2.5, 5, 10, and 15 mol% cross-linker at 60°C.

membranes in this study are listed in Table I. All of the membranes, with the exception of GT64-2.5, have an ASR less than or equal to 0.04 Ω-cm², which exceeds the ARPA-E IONICS (US Department of Energy) goal for fuel cell integration. Table I also shows how modest cross-linking in these polymers greatly decreased the water uptake. The swelling decreased to only 7% and high conductivity was achieved without excessive water, as shown by the decreasing WU/ASR values. It is noted that achieving high conductivity by increasing WU can lead to poor mechanical stability for the membrane and devices made from those membranes.

Two sets of fuel cells were constructed using the reinforced membranes from Table I. The first set of fuel cells was operated with humidified H_2 and O_2 reacting gases, with the electrode deposited onto 5% wetproofed Toray-H-60 GDLs, at a cell temperature of 60°C. This results from this set of experiments are summarized in Table II. After a short break-in period where the anode and cathode RH were optimized, forward and reverse polarization scans were run on each cell to determine peak power density. The optimized anode and cathode dew points are listed in Table II using the notation (A/C), where the value of A represents the anode dew point and the value of C represents the cathode dew point in degrees Celsius. This notation will be used throughout this paper. The power density and polarization curves for the cells with various TMHDA content in the AEM are shown in Figure 2. The cell voltage at peak power for all samples at 60°C was ca. 0.55 V. The specific power and specific current values were calculated based on the peak power density, current produced at peak power, and the metal loading of the electrodes.

Generally, the peak power density increased with TMHDA concentration, although the peak power output for 0 and 2.5 mol% TMHDA, and 5 and 10 mol% TMHDA were very similar, Table II and Figure 2. Among the membranes tested, the lowest performing cells used membranes with 0 and 2.5 mol% TMHDA; 1.24 to 1.39 W/cm² peak power, respectively. Intermediate power levels were recorded for membranes with 5 and 10 mol% TMHDA: 1.89 and 1.90 W/cm², respectively. The highest peak power density was observed for the cell containing the GT64-15 membrane: 2.20 W/cm². Even at 60°C, this cell exceeded the previous best literature value for AEM fuel cell reported by Wang et al., which achieved 2.0 W/cm² at 80°C.[20]

At 80°C, the performance of the fuel cells significantly increased, as shown in Figure 3 and summarized in Table III. Membranes with 10 and 15 mol% TMHDA were selected for testing at 80°C because of their higher performance. The GDEs used in these tests and the testing method were slightly modified compared to the 60°C experiments. Most notably, the catalyst layers were deposited onto Toray-H-60 with 20% wetproofing, and the dew point of the anode and cathode feed gases were more finely optimized. As shown in Figure 3, there is less separation in power density among the four cells tested, and the power density produced is similar across a wide range of TMHDA concentrations. Just like the 60°C experiments, the cells achieved peak power at ca. 0.54 V. Both GT64-10 and GT64-20 achieved a peak power density
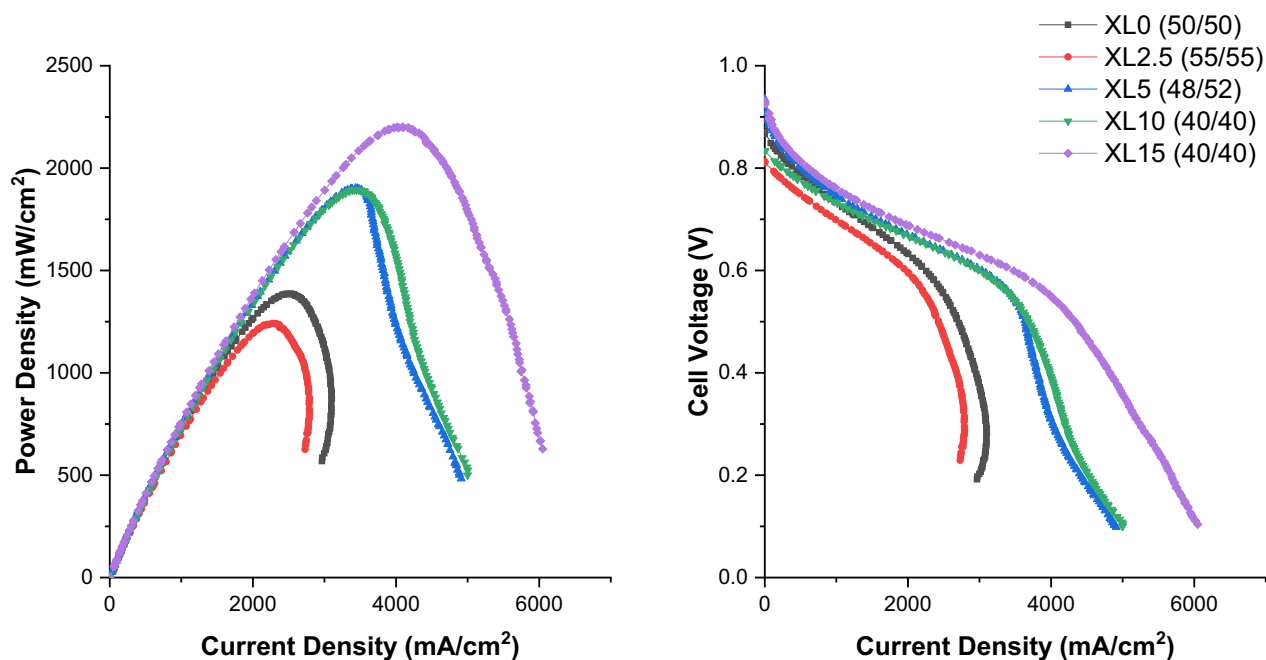
Figure 2. Comparison of peak performance after RH optimization. Cell temperature for all samples was 60°C.
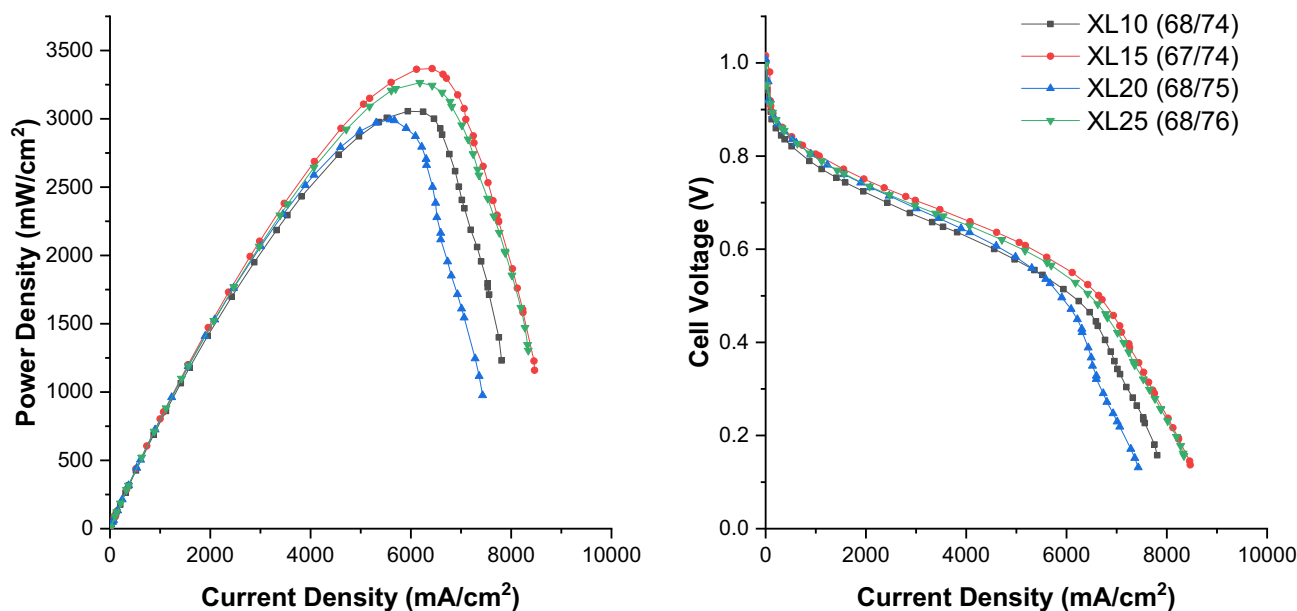
Figure 3. Comparison of peak performance after RH optimization. Cell temperature for all samples was 80°C.

of ca. 3.0 W/cm² with similar optimal anode and cathode dew points. The peak power for GT64-25 was 3.27 W/cm². Similar to the results obtained at 60°C, GT64-15 showed the highest performance among all membranes tested with a peak power density of 3.37 W/cm². To the authors' knowledge, this is the highest performance reported for an AEM fuel cell to date, surpassing the previous record by 70%.[20] It is interesting to note that the peak power density occurred with a membrane which did not have the highest hydroxide conductivity. GT64-5 had a higher conductivity than GT64-15.[7] This shows the disruptive nature of excessive WU and swelling, and the subtle interactions between conductivity, mechanical deformation and current density. Conductivity alone does not capture the deleterious effects of mechanical deformations on cell performance. The achieved power density appears to be the result of off-setting trends of mechanical stability (better with higher TMHDA concentration) and lower conductivity, both of which may be related to lower WU.

The water uptake normalized by the ASR (WU/ASR) and the IEC normalized by the ASR (IEC/ASR), Table I, give insight into why certain TMHDA concentrations are better than others. The ASR normalized IEC, IEC/ASR, is similar to conductivity per IEC (σ/IEC), which has been used to measure mobility or how efficient ion conducting groups are for transporting hydroxide ions.[7–9,11] For membranes in this study, the ion conduction efficiencies are all quite similar, ranging from 3.20 to 3.33. This is because there are only slight variations in the ASR and IEC among the samples tested. An additional parameter is WU/ASR, which shows that although the hydroxide conductivity

decreased with TMHDA concentration, cell performance did not suffer much because the lower WU (and resulting swelling) was beneficial.

One potential concern with the use of thin composite membranes is hydrogen crossover. Prior to the break-in procedure, a hydrogen crossover test was performed by flowing H₂ at the negative electrode (anode) and N₂ at the positive electrode (cathode). The hydrogen crossover current was measured by applying a voltage of 0.5 V across the cell and the resulting values are listed in Table II. The hydrogen crossover was 5 to 54 mA/cm² and did not correlate with membrane thickness or cross-linker concentration, as would have been expected. From these results, it is suspected that crossover measurements may have been influenced by unintentional thin points or fabrication defects in the membranes, although no obvious regions were seen. The effect of the elevated crossover for GT64-10 can be seen in the lower OCV values. The OCV ranged from 0.881 V to 0.950 V. Other fuel cells using similar electrode formulations had OCV values of ca. 1.1 V.[19,20]

The relative humidities of the anode and cathode feeds are known to play a critical role in alkaline exchange membrane fuel cell performance.[16] The water content in the hydrogen and oxygen input streams must be carefully balanced with the production of water at the anode, the diffusion of water through the membrane, and consumption of water at the cathode. Factors such as catalytic activity and loading can affect each electrode differently, which in turn affects the overall cell performance. As mentioned earlier, the three tiers of power output can be seen in Figure 2 based on the TMHDA concentration in the membrane. However, there is an additional trend that can be

Table III. Fuel cell performance highlights at 80°C.

XL (mol%)	OCV (V)	A/C dew point (°C)	HFR (mΩ)[a]	Cell potential (V)	CD (mA/cm²)	PPD (W/cm²)	PtRu/C loading (mg/cm²)	Pt/C loading (mg/cm²)	Spec. power (W/mg PtRu)	Spec. power (W/mg Pt)	Spec. current (mA/mg PtRu)	Spec. current (mA/mg Pt)
10	1.001	68/74	7.01	0.514	5940	3.06	0.70	0.60	4.36	5.09	8491	9906
15	1.016	67/74	5.05	0.524	6425	3.37	0.70	0.60	4.81	5.61	9182	10712
20	1.009	68/75	1.52	0.536	5588	3.00	0.70	0.60	4.28	4.99	7982	9313
25	0.996	68/76	5.74	0.528	6179	3.27	0.70	0.60	4.66	5.44	8834	10307

[a]High frequency resistance measured by EIS; All other values measured or calculated based on test station data. XL = cross-linker concentration; A/C = denotes anode (A) and cathode (C) dew points in degrees Celsius, respectively; CD = current density; PPD = peak power density.
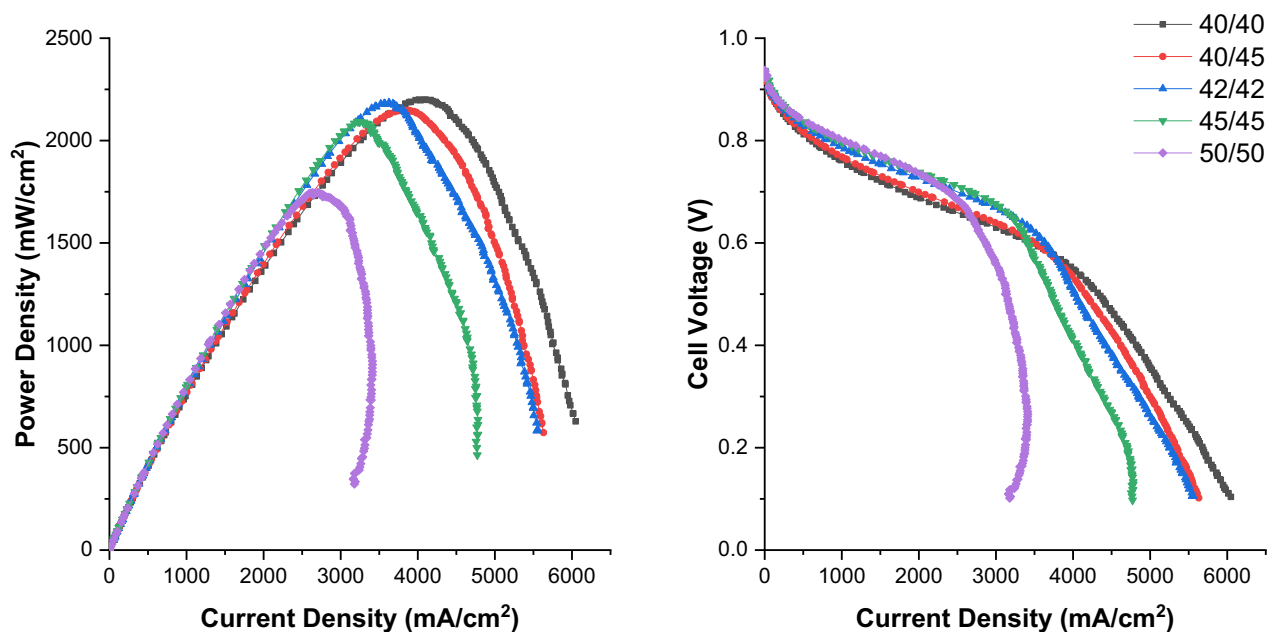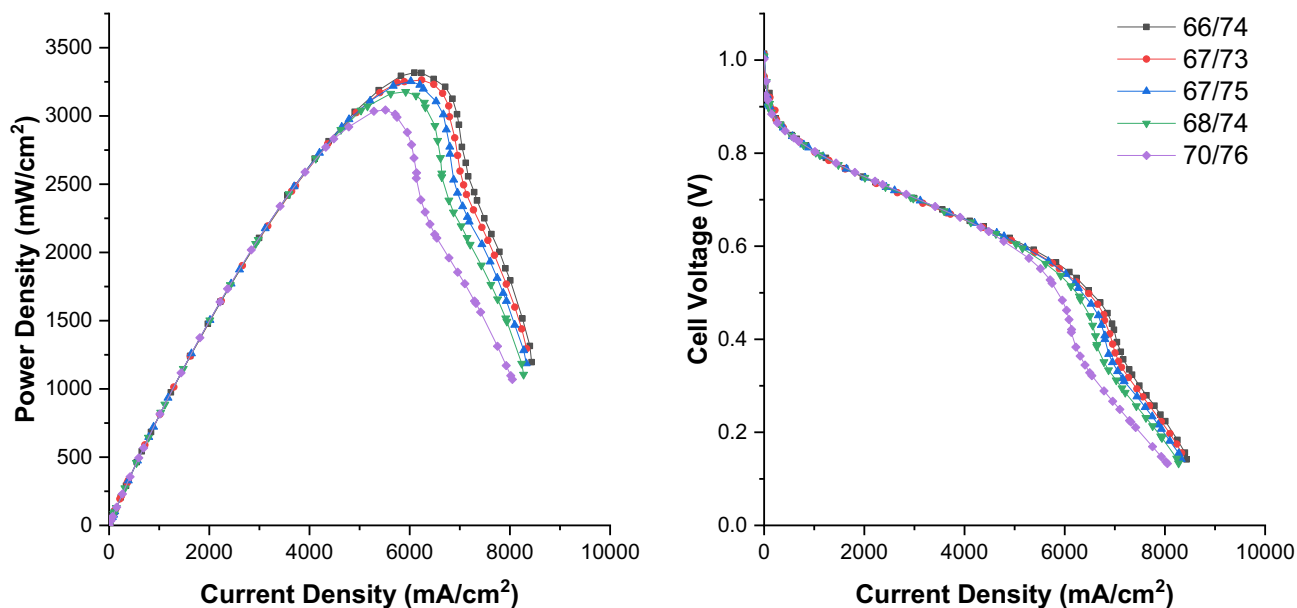
Figure 4. Polarization curves for GT64-15 at cell temperature of 60°C with various anode and cathode inlet dew points.

seen in this data. Not only did the performance go up with TMHDA concentration, but the amount of water fed to the cell in the reacting gases decreased (i.e. lower dew points). As reported previously, water uptake decreases with increasing TMHDA concentration in the polymer network.[7] As seen in the WU data in Table I, the higher TMHDA concentration decreased the WU. However the tighter and more rigid polymer network also appears to lock water inside the membrane, limiting the rate of dry-out.

The cells with ≥10 mol% TMHDA concentration operated at 60°C had a peak power density with anode and cathode dew points both at 40°C. Figure 4 shows the RH optimization for the GT64-15 membrane at 60°C cell temperature. At anode and cathode dew points of 50°C, there is clearly too much water in the system, which causes electrode flooding and lower power. The performance increased steadily

as the humidity was reduced to a dew point of 40°C for both feed streams. This trend continued for an intermediate TMHDA concentration (5 mol%), where the dew points at the highest peak power density were 48°C for the anode and 52°C for the cathode. At TMHDA concentration of ≤2.5 mol%, the best performance was achieved when the dew points for the anode and cathode were both at 50°C. The inlet RH trends for GT64-2.5 and GT64-0 can be seen in Figs. S1 and S2 of the Supporting Information. Another interesting trend from the optimization data in Figure 4 is that the mass transport limited current increased with decreasing reacting gas dew points. This is a clear sign that water transport is performance-limiting during AEM fuel cell operation.

RH sensitivity was also investigated at a cell temperature of 80°C. Figure 5 shows the RH optimization at 80°C for an AEM fuel cell operated at 80°C with a GT64-15 membrane. Although the overall

Figure 5. Polarization curves for GT64-15 at cell temperature of 80°C with various anode and cathode inlet dew points.
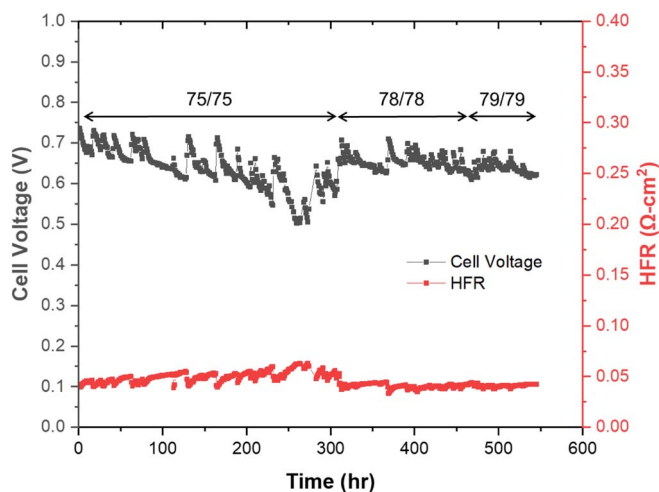
Figure 6. Cell voltage and HFR of GT64-15 over time at 80°C under H_2 and CO_2-free air.

water content at the inlet is higher at this elevated temperature, the same trend was observed. At 80°C, water has a higher vapor pressure so the membrane dries out at a faster rate, thus requiring higher humidity in the feed streams. For a cross-linker concentration of 15 mol%, the cell performance benefited from lower anode and cathode dew points than the operating temperature, 66°C and 74°C, respectively. The effect of cell flooding can be seen starting at inlet dew points of 68°C and 74°C (anode and cathode, respectively) and became more severe at 70°C and 76°C (anode and cathode, respectively).

The fuel cells were generally operated for 24 h to ensure that dependable performance values were obtained and the AEMs had good stability in the highly alkaline environment. One long-term AEM fuel cell stability test was performed with the GT64-15 membrane at 80°C using CO_2-free air and electrodes deposited onto a 5% wetproofed GDL. The polarization curve was recorded prior to switching to CO_2-free air, as shown in Figure S3 of the Supporting Information. Figure S3 shows the current-voltage curve using hydrogen and oxygen as the feed gasses. This cell was not fully optimized for the highest power density (like later cells) and its power density at 0.7 V was 1450 mW/cm². It is noted that even though this is not the highest power cell in this study, the peak power was about 2.3 W/cm², which still exceeds the highest published cell to-date. This cell was selected for long-term aging and Figure 6 shows hourly data of the cell voltage vs. time at constant current, 600 mA/cm². It is noted that the cell power dropped to 31% of its H_2/O_2 value when air was used in place of oxygen. This reflects the lower activity of oxygen in air and also the importance of optimizing the electrode structure and relative humidity of the feed gas. These effects are currently under investigation and may be the subject of future reports. The cell ran for 545 h without detectable membrane degradation, at which point the experiment was terminated. During the first 300 hours, the cell performance dropped by about 17%. This change in performance was likely caused by the cell water dynamics, where a net loss of water slowly occurred at the electrode over time, as evidenced by the increasing ASR. As such, the dew points of the anode and cathode were adjusted to 78°C at the 300 h point to increase the water content in the cell. This increase in dew point restored the cell to its initial level of performance. After operating for an additional 150 h, the dew points of the anode and cathode were both increased to 79°C and were held there for the remainder of the durability test. The cause of the change in the MEA that necessitated a higher dew point is not clear at this time. After adjusting the water content, the cell voltage and the HFR also returned to their initial values showing that proper hydration had been restored. The initial and final HFR values (0.043 Ω-cm² and 0.042 Ω-cm², respectively) were essentially the same showing that the AEM conduction

properties did not change substantially and the membranes had very high in situ stability.

Summary

The behavior of high IEC, high conductivity AEMs were analyzed and used in alkaline H_2/O_2 fuel cells. The membranes were composed of a reinforced poly(norbornene) BCP. It was found that light cross-linking provided critical mechanical stability so that very high IEC could be used without penalty of excessive water uptake and swelling. The improvement in full-cell performance was greater than simply minimizing the membrane ohmic losses. Mechanical stability of the membrane and electrode/membrane interface is exceedingly important to the efficient transport of ions within the cell. The fuel cells were sensitive to the relative humidity of the feed gases, and the reacting gas dew points needed to be optimized to yield the highest peak power. The optimum AEM (15 mol% TMHDA crosslinker) and cell operating conditions resulted in a peak power density of 3.4 W/cm² at 80°C, the highest reported to-date. It was also shown that the AEMs were stable for long periods of time (>500 h) under load with no change in the membrane resistance.

ORCID

Mrinmay Mandal ⓘ https://orcid.org/0000-0002-3404-9588
William E. Mustain ⓘ https://orcid.org/0000-0001-7804-6410
Paul A. Kohl ⓘ https://orcid.org/0000-0001-6267-3647

References

1. B. C. H. Steele and A. Heinzel, *Nature*, **414**, 345 (2001).
2. G. F. McLean, T. Niet, S. Prince-Richard, and N. Djilali, *International Journal of Hydrogen Energy*, **27**, 507 (2002).
3. D. R. Dekel, *Journal of Power Sources*, **375**, 158 (2018).
4. J. R. Varcoe, R. C. T. Slade, G. L. Wright, and Y. Chen, *The Journal of Physical Chemistry B*, **110**, 21041 (2006).
5. J. R. Varcoe, P. Atanassov, D. R. Dekel, A. M. Herring, M. A. Hickner, P. A. Kohl, A. R. Kucernak, W. E. Mustain, K. Nijmeijer, K. Scott, T. Xu, and L. Zhuang, *Energy & Environmental Science*, **7**, 3135 (2014).
6. S. Gottesfeld, D. R. Dekel, M. Page, C. Bae, Y. Yan, P. Zelenay, and Y. S. Kim, *Journal of Power Sources*, **375**, 170 (2018).
7. M. Mandal, G. Huang, and P. A. Kohl, *ACS Applied Energy Materials*, **2**, 2447 (2019).
8. W. Chen, M. Mandal, G. Huang, X. Wu, G. He, and P. A. Kohl, *ACS Applied Energy Materials*, **2**, 2458 (2019).
9. M. Mandal, G. Huang, and P. A. Kohl, *Journal of Membrane Science*, **570–571**, 394 (2019).
10. H.-S. Dang and P. Jannasch, *Journal of Materials Chemistry A*, **4**, 11924 (2016).
11. L. Liu, G. Huang, and P. A. Kohl, *Journal of Materials Chemistry A*, **6**, 9000 (2018).
12. L. Liu, J. Ahlfield, A. Tricker, D. Chu, and P. A. Kohl, *Journal of Materials Chemistry A*, **4**, 16233 (2016).
13. M. Mamlouk, J. A. Horsfall, C. Williams, and K. Scott, *International Journal of Hydrogen Energy*, **37**, 11912 (2012).
14. L. Zhu, T. J. Zimudzi, N. Li, J. Pan, B. Lin, and M. A. Hickner, *Polymer Chemistry*, **7**, 2464 (2016).
15. L. Wang, J. J. Brink, and J. R. Varcoe, *Chemical Communications*, **53**, 11771 (2017).
16. T. J. Omasta, L. Wang, X. Peng, C. A. Lewis, J. R. Varcoe, and W. E. Mustain, *Journal of Power Sources*, **375**, 205 (2018).
17. T. J. Omasta, X. Peng, H. A. Miller, F. Vizza, L. Wang, J. R. Varcoe, D. R. Dekel, and W. E. Mustain, *J Electrochem Soc*, **165**, J3039 (2018).
18. L. Wang, E. Magliocca, E. L. Cunningham, W. E. Mustain, S. D. Poynton, R. Escudero-Cid, M. M. Nasef, J. Ponce-González, R. Bance-Souahli, R. C. T. Slade, D. K. Whelligan, and J. R. Varcoe, *Green Chemistry*, **19**, 831 (2017).

19. T. J. Omasta, A. M. Park, J. M. LaManna, Y. Zhang, X. Peng, L. Wang, D. L. Jacobson, J. R. Varcoe, D. S. Hussey, B. S. Pivovar, and W. E. Mustain, *Energy & Environmental Science*, **11**, 551 (2018).
20. L. Wang, M. Bellini, H. A. Miller, and J. R. Varcoe, *Journal of Materials Chemistry A*, **6**, 15404 (2018).
21. T. P. Pandey, A. M. Maes, H. N. Sarode, B. D. Peters, S. Lavina, K. Vezzù, Y. Yang, S. D. Poynton, J. R. Varcoe, S. Seifert, M. W. Liberatore, V. Di Noto, and A. M. Herring, *Physical Chemistry Chemical Physics*, **17**, 4367 (2015).
22. J. Ahlfield, G. Huang, L. Liu, Y. Kaburagi, Y. Kim, and P. A. Kohl, *J Electrochem Soc*, **164**, F1648 (2017).
23. J. Pan, C. Chen, Y. Li, L. Wang, L. Tan, G. Li, X. Tang, L. Xiao, J. Lu, and L. Zhuang, *Energy & Environmental Science*, **7**, 354 (2014).
24. J. Wang, S. Gu, R. Xiong, B. Zhang, B. Xu, and Y. Yan, *ChemSusChem*, **8**, 4229 (2015).
25. D.-Y. Park, P. A. Kohl, and H. W. Beckham, *The Journal of Physical Chemistry C*, **117**, 15468 (2013).
26. L. Wang and M. A. Hickner, *Soft Matter*, **12**, 5359 (2016).
27. Y. Li, Y. Liu, A. M. Savage, F. L. Beyer, S. Seifert, A. M. Herring, and D. M. Knauss, *Macromolecules*, **48**, 6523 (2015).
28. C. Chen, J. Pan, J. Han, Y. Wang, L. Zhu, M. A. Hickner, and L. Zhuang, *Journal of Materials Chemistry A*, **4**, 4071 (2016).
29. A. D. Mohanty, S. E. Tignor, J. A. Krause, Y.-K. Choe, and C. Bae, *Macromolecules*, **49**, 3361 (2016).
30. A. D. Mohanty and C. Bae, *Journal of Materials Chemistry A*, **2**, 17314 (2014).
31. C. G. Arges and L. Zhang, *ACS Applied Energy Materials*, **1**, 2991 (2018).
32. J. Pan, Y. Li, J. Han, G. Li, L. Tan, C. Chen, J. Lu, and L. Zhuang, *Energy & Environmental Science*, **6**, 2912 (2013).
33. M. R. Hibbs, *Journal of Polymer Science Part B: Polymer Physics*, **51**, 1736 (2013).
34. L. Liu and P. A. Kohl, *Journal of Polymer Science Part A: Polymer Chemistry*, **56**, 1395 (2018).
35. S. Martínez-Arranz, A. C. Albéniz, and P. Espinet, *Macromolecules*, **43**, 7482 (2010).
36. G. Merle, M. Wessling, and K. Nijmeijer, *Journal of Membrane Science*, **377**, 1 (2011).
37. E. Quartarone, S. Angioni, and P. Mustarelli, *Materials (Basel, Switzerland)*, **10**, 687 (2017).
38. F. Zhang, H. Zhang, J. Ren, and C. Qu, *Journal of Materials Chemistry*, **20**, 8139 (2010).
39. Y. Zhao, H. Yu, D. Yang, J. Li, Z. Shao, and B. Yi, *Journal of Power Sources*, **221**, 247 (2013).
40. S. D. Poynton, R. C. T. Slade, T. J. Omasta, W. E. Mustain, R. Escudero-Cid, P. Ocón, and J. R. Varcoe, *Journal of Materials Chemistry A*, **2**, 5124 (2014).